Third AO4ELT Conference - Adaptive Optics for Extremely Large Telescopes
Florence, Italy. May 2013
ISBN: 978-88-908876-0-4
DOI: 10.12839/AO4ELT3.13290

WAVE-FRONT RECONSTRUCTION FOR THE NON-LINEAR CURVATURE WAVE-FRONT SENSOR

Carlos Correia[1,a], J.-P. Véran[2], and O. Guyon[3] and C. Clergeon[3]

[1] CAUP – Centre for Astrophysics University of Porto, Porto, Portugal
[2] National Research Council, Herzberg Institute of Astrophysics, Victoria, Canada
[3] Subaru Telescope, National Observatory of Japan, Hilo, Hawaii, USA

Abstract. Non-linear curvature wave-front sensing (nlCWFS) delivers outstanding sensitivity and high dynamic range by lifting the linearity constraint of standard curvature wave-front sensing and working in the non-linear Fresnel (near-field) regime [Guyon, 2010].
The goals of this paper are twofold: 1) revisit the phase-diversity `PD` formalism and attempt to use this framework, originally developed for the Fraunhofer (far-field) regime, with `nlCWFS` signals and 2) develop formulae making explicit use of the Fresnel regime for later use with gradient-based non-linear minimisation methods.

1 Curvature wave-front sensing: linear and non-linear regimes

The highly sensitive non-linear curvature wave-front sensing (`nlCWFS`) takes full advantage of diffraction, which encodes wave-front aberrations into patterns of diffraction-limited interference speckles [Guyon, 2010]. To do so, a set of images are acquired away from the pupil-plane, beyond the linear regime used in traditional linear curvature WFS, but not reaching the Fraunhofer regime used in phase-diversity (`PD`).

In `nlCWFS` images are acquired in the intermediate regime at locations that optimise the sensitivity to a large range of spatial frequencies. The trade is set by a non-linear wave-front reconstruction process which involves computationally intensive non-linear algorithms. One such example is the Gerchberg-Saxton iterative algorithm proposed originally in [Guyon, 2010].

The linear, non-linear and Phase Diversity techniques are thus linked by the same principle of acquiring multiple images at different propagation distances and work from there to reconstruct the phase. The differences lie on the locations of the planes where those images are acquired.

To enforce linearity linear CWFS uses largely defocused images that correspond to distances closer to the pupil-plane [Roddier and Roddier, 1993],[Guyon et al., 2008].

On the other hand, `PD` relies on a forward model of image formation using the far-field (Fraunhofer) approximation thus operating near the focal plane where the defocus terms are small. [Fienup et al., 1998] gives a thorough account of the similarities between `PD` and `linCWFS` . The massive computation required makes its use more amenable to non-real-time applications, as is the case of non-common path aberration estimation.

In this paper we investigate approximations that could allows us to use the framework developed for phase-diversity (`PD`) to compute the maximum a-posteriori (MAP) wave-front estimate [Correia, 2013]. Since the latter proves insufficient, we use instead a minimisation criterion that explicitly uses the image formation model in the near-field (Fresnel) regime and derive its partial

[a] ccorreia@astro.up.pt, Formerly with HIA

derivatives with respect to the parameters of the wave-front, expanded onto a Zernike polynomial basis of functions.

At present, only the mono-chromatic case is dealt with.

2 Image formation models

The incoherent image formation model is approximated by a cyclic discrete convolution

$$i_k(\mathbf{x},\boldsymbol{\alpha}) = \sum_{\mathbf{x}'\in\Omega} o(\mathbf{x}')s_k(\mathbf{x}-\mathbf{x}',\boldsymbol{\alpha}) + \eta_k(\mathbf{x}) = o(\mathbf{x}) * s_k(\mathbf{x},\boldsymbol{\alpha}) + \eta_k(\mathbf{x}) \tag{1}$$

where $i_k(\mathbf{x},\boldsymbol{\alpha})$ the k^{th} image, $o(\mathbf{x})$ is the object, $s(\mathbf{x},\boldsymbol{\alpha})$ is an indicial response function, $\eta(\mathbf{x})$ is additive noise and $*$ represents 2-D convolution. Variables in the pupil and image planes are indexed by $\mathbf{r}$ and $\mathbf{x}$ respectively[1].

The pupil-plane wave-front aberrations are parametrised as

$$\varphi(\mathbf{r},\boldsymbol{\alpha}) = \sum_{j=1}^{J} \alpha_j \psi(\mathbf{r}) \tag{2}$$

with J coefficients in the set, $\psi(\mathbf{r})$ an appropriate set of basis functions. In what follows we use the Zernike polynomials [Noll, 1976].

2.1 Image formation model in the far-field

In the far-field regime, the Fraunhofer approximation applies. The indicial response function from Eq. (1) is the the point-spread function (PSF)

$$i_k(\mathbf{x},\boldsymbol{\alpha}) = \underbrace{\left|\mathbf{FT}^{-1}\left\{H_k(\mathbf{r},\boldsymbol{\alpha})\right\}(\mathbf{x})\right|^2}_{s_k^{\mathrm{Fh}}(\mathbf{x},\boldsymbol{\alpha})} * o(\mathbf{x}) + \eta_k(\mathbf{x}) \tag{3}$$

where $H_k(\mathbf{r},\boldsymbol{\alpha}) = |H_k(\mathbf{r},\boldsymbol{\alpha})|\exp\{i\varphi(\mathbf{r},\boldsymbol{\alpha}) + \theta_k(\mathbf{r})\}$ is a generalised pupil function (with or without apodisation). The PSF is thus

$$s_k^{\mathrm{Fh}}(\mathbf{x},\boldsymbol{\alpha}) = \left|\mathbf{FT}^{-1}\left\{|H_k(\mathbf{r},\boldsymbol{\alpha})|\exp\left[i\varphi(\mathbf{r},\boldsymbol{\alpha}) + i\theta_k(\mathbf{r})\right]\right\}(\mathbf{x})\right|^2 = |h_k(\mathbf{x},\boldsymbol{\alpha})|^2 \tag{4}$$

in which $\mathbf{FT}^{-1}$ is the inverse Fourier transform, and $\theta_k(\mathbf{r})$ is a diversity term for the k^{th} image.

2.2 Image formation model in the near-field

For finite propagation distances the use of the PSF in Eq. (3) no longer holds. Instead the near-field Fresnel propagation is required, according to which the image model becomes

$$i_k(\mathbf{x},\boldsymbol{\alpha}) = \underbrace{\left||H(\mathbf{r})|\exp\left[i\varphi(\mathbf{r},\boldsymbol{\alpha})\right] * \frac{1}{i\lambda z_k}\exp\left(\frac{i\pi}{\lambda z_k}|\mathbf{r}|^2\right)\right|^2}_{s_k^{\mathrm{Fn}}(\mathbf{x},\boldsymbol{\alpha})} * o(\mathbf{x}) + \eta_k(\mathbf{x}) \tag{5}$$

[1] Following [Paxman et al., 1992], the image plane, pupil-plane and OTF plane are defined over Ω that assumes different supports as a function of the variables it is linked to. With some abuse of notation, it is used here more loosely and indistinctly.

where

$$s_k^{\mathrm{Fn}}(\mathbf{x},\boldsymbol{\alpha}) \triangleq |H(\mathbf{r}) * P_k(\mathbf{r})|^2 \tag{6}$$

with the Fresnel propagator to the k^{th}-plane $P_k(\mathbf{r})$

$$P_k(\mathbf{r}) \triangleq \frac{1}{i\lambda z_k}\exp\left(\frac{i\pi}{\lambda z_k}|\mathbf{r}|^2\right) \tag{7}$$

3 Wave-front reconstruction with gradient-based minimisation methods

3.1 Criterion

Consider the following criterion

$$L(o,\boldsymbol{\alpha},\gamma) = \sum_{k=1}^{K}\mu_k\left\|i_k - \underbrace{o * s_k(\varphi(\boldsymbol{\alpha}))}_{model}\right\|^2_{L_2(\Omega)} + \gamma\varphi(\boldsymbol{\alpha})^{\mathsf{T}}\mathbf{R}\varphi(\boldsymbol{\alpha}) \tag{8}$$

with μ_k a term linked to the inverse of the noise variance in each image and $\gamma\varphi(\boldsymbol{\alpha})^{\mathsf{T}}\mathbf{R}\varphi(\boldsymbol{\alpha})$ is a regularisation term involving the inverse covariance matrix of the phase parameters $\mathbf{R} \triangleq \left\langle\varphi(\boldsymbol{\alpha})\varphi(\boldsymbol{\alpha})^{\mathsf{T}}\right\rangle^{-1}$, with γ a tunable parameter.

3.2 Wave-front reconstruction using the PD framework

Assuming equal noise variance on all images, the likelihood term in Eq. (8) can be written

$$L^{\mathrm{LH}}(o,\boldsymbol{\alpha}) \propto \sum_{k=1}^{K}\sum_{\mathbf{x}\in\Omega}[i_k(\mathbf{x}) - o(\mathbf{x}) * s_k(\mathbf{x},\boldsymbol{\alpha})]^2 \tag{9}$$

It is convenient to express the Fourier-transformed criterion of Eq. (8) using the Parseval theorem to recast the minimisation in the OTF plane instead. One thus gets (capital letters used for Fourier-transformed variables)

$$L^{\mathrm{LH}}(o,\boldsymbol{\alpha}) \propto \frac{1}{N^2}\sum_{k=1}^{K}\sum_{\mathbf{r}\in\Omega}|I_k(\mathbf{r}) - O(\mathbf{r})S_k(\mathbf{r},\boldsymbol{\alpha})|^2 \tag{10}$$

When in the PD regime, *i.e.* $s_k = s_k^{\mathrm{Fh}}$, [Paxman et al., 1992] provides the explicit OTF-plane criteria and its derivatives for the joint estimation of the object and aberration parameters.

We note that in AO, the object is a point-source and thus, joint optimisation may be discarded providing for an easier derivation. Albeit, estimating the object has a smoothing effect on the estimates and may be thus preferable.

3.3 Wave-front reconstruction using a custom `nlCWFS` framework

Consider the criterion of Eq. (9), with $s_k(\mathbf{x}, \boldsymbol{\alpha}) = s_k^{\mathrm{Fn}}(\mathbf{x}, \boldsymbol{\alpha})$ from Eq. (6). We proceed by computing the criterion and its derivatives in the image-plane. Under the assumption that the object is known to be a point-source, then we get

$$\begin{aligned}\frac{\partial}{\partial\alpha_j}L^{\mathrm{LH}}(\boldsymbol{\alpha}) &= \sum_{k=1}^{K} -2\frac{\partial}{\partial\alpha_j}i_k(\mathbf{x})\left[o(\mathbf{x}) * s_k^{\mathrm{Fn}}(\mathbf{x},\boldsymbol{\alpha})\right] + 2\left(\frac{\partial}{\partial\alpha_j}\left[o(\mathbf{x}) * s_k^{\mathrm{Fn}}(\mathbf{x},\boldsymbol{\alpha})\right]\right)\left[o(\mathbf{x}) * s_k^{\mathrm{Fn}}(x,\boldsymbol{\alpha})\right] \\ &= \sum_{k=1}^{K} -2i_k(\mathbf{x})\left[o(\mathbf{x}) * \frac{\partial}{\partial\alpha_j}s_k^{\mathrm{Fn}}(\mathbf{x},\boldsymbol{\alpha})\right] + 2\left[o(\mathbf{x}) * \frac{\partial}{\partial\alpha_j}s_k^{\mathrm{Fn}}(\mathbf{x},\boldsymbol{\alpha})\right]\left[o(\mathbf{x}) * s_k^{\mathrm{Fn}}(\mathbf{x},\boldsymbol{\alpha})\right]\end{aligned} \tag{11}$$

where the partial derivatives of the Fresnel propagator with respect to the parameters of the wave-front are

$$\begin{aligned}\frac{\partial}{\partial\alpha_j}s_k^{\mathrm{Fn}}(\mathbf{x},\boldsymbol{\alpha}) &= \frac{\partial}{\partial\alpha_j}\left|H(\mathbf{r}) * P_k(\mathbf{r})\right|^2 \\ &= 2\Re\left\{\left(i\varphi_j H(\mathbf{r}) * P_k(\mathbf{r})\right)\left(H(\mathbf{r}) * P_k(\mathbf{r})\right)^*\right\}\end{aligned} \tag{12}$$

A star in supperscript represents conjugate.

3.4 Computational demand

As it stands, for real-time application, the `nlCWFS` requires a number of 2-D Fourier transforms (FFT) per iteration that is proportional to KJ, the product of the number of images by the number of wave-front parameters. As a comparison, the Gerchberg-Saxton (`GS`) requires an amount per iteration that is proportional to K, the same with `PD`.

Thus for real-time application the dependence of the number of 2-D FFTs on J makes the explicit criterion minimisation very demanding. Following [Paxman et al., 1992], we expect some degree of simplification from using a zonal representation of phase instead of the current Zernike polynomials – for `PD` this lifts the J dependence and is thus a path to explore. Several other convergence acceleration approaches can be considered, involving a linear approximation under the low phase aberrations scenario, for all or a part of the modes and/or a hierarchical (multi-resolution) method.

As a parallel development, we note that the appealing MAP structure of the criteria and the existence of closed-form partial derivatives has its counterpart on the `GS` as well. The latter is less prone to remain trapped in local minima [Fienup, 1982] and could be used jointly with an approximate linear model to short-circuit slow convergence (or plateaus) when far from the solution – see Fig. 3.

4 Criteria evaluation

We use simulations for a 8 m telescope with 4 planes located at $\pm 2500, 3500$ km from the pupil at $\lambda = 0.64\,\mu m$, 128-pixel images with photon-noise on/off.

4.1 `nlCWFS` WFR using the `PD` framework

A first attempt is to use the `PD` framework with `nlCWFS` signals. For that, the defocus terms are adjusted to the propagation at which the 4 `nlCWFS` planes are located.

Propagating to a distance z_k is equivalent as defocusing the optical system by [Mahajan, 1998]

$$\theta_{z=z_k} \propto \frac{\pi D^2}{4\lambda z_k} \qquad [rad p.v.] \tag{13}$$

radians peak-to-valley. In Eq. (13), D is the telescope diameter and λ the sensing wavelength.

Thus, we model images using Eq. (3) which becomes

$$\begin{aligned} i_{z=z_k}(\mathbf{x},\boldsymbol{\alpha}) &= s_k^{\mathrm{Fh}}(\mathbf{x},\boldsymbol{\alpha}) * o(\mathbf{x}) + \eta_k(\mathbf{x}) \\ &= \left|\mathbf{FT}^{-1}\left\{|H_k(\mathbf{r},\boldsymbol{\alpha})| \exp\left[i\varphi(\mathbf{r},\boldsymbol{\alpha}) + i\theta_{z=z_k}(\mathbf{r})\right]\right\}(\mathbf{x})\right|^2 * o(\mathbf{x}) + \eta(\mathbf{x}) \end{aligned} \tag{14}$$

where $\theta_{z_k}(\mathbf{r})$ is a pure defocus aberration with radians peak-to-valley in Eq. (13).

Figure 1 compares 4 cases: known or estimated object against the computation of the criterion in two variants: either with the OTF computed formally from the PSF or from the Fourier-transformed Fresnel intensity pattern obtained at K finite distances. Estimating the object circumvents the model approximation we are proposing here.

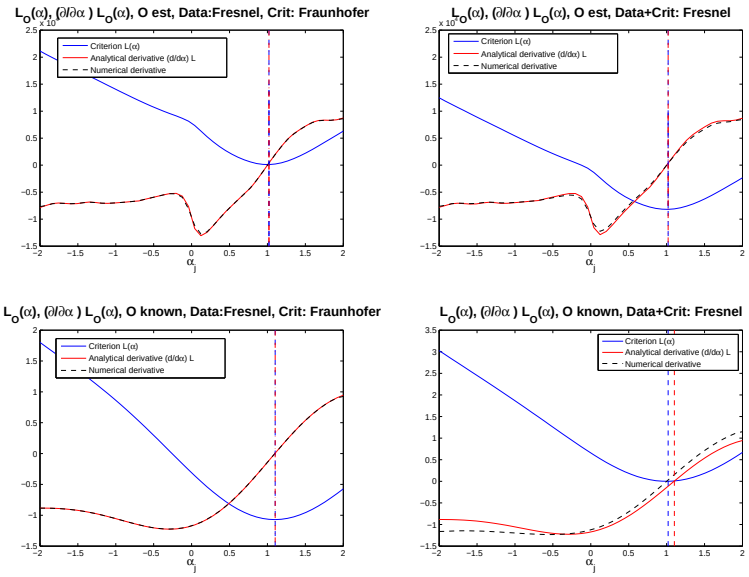

Fig. 1. Criterion and its derivatives when the images are obtained by Fresnel propagation. $K = 4$. True coefficient $\alpha_5 = 1$.

However, this quick attempt proved insufficient to work in the multi-mode case, when noise is added to the measurements. We further note that even in closed-loop the convergence is slow with overall performance far from the one obtained with the `GS` algorithm.

4.2 `nlCWFS` WFR using proper criterion derivatives

The criterion and its derivatives are now computed using a forward model that involves explicitly the image formation in the Fresnel regime – Eq. (5).

Figure 2 compares the analytical and numerical derivatives which are in perfect agreement with the numerical ones.

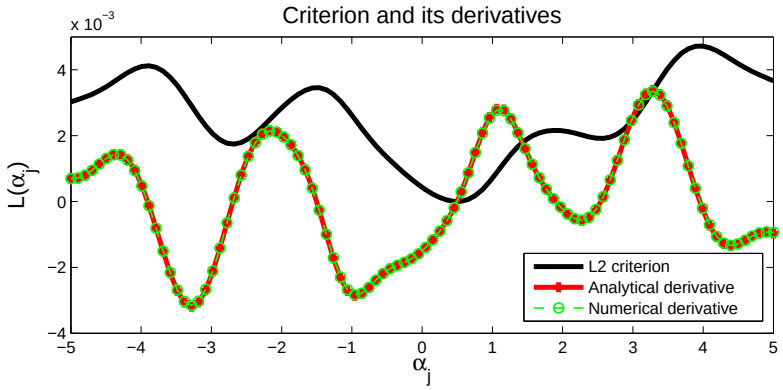

Fig. 2. Example of the criterion and its derivatives using Eq. (9) and Eq. (11). $K = 4$. True coefficient $\alpha_{22} = 0.5$ rad, chosen to provide for an easier visual inspection of the many local minima.

We've checked the existence of multiple minima for a large number of modal functions and observed the presence of several pathological cases (as the one provided in the example). Therefore, despite a more accurate model, in order to guarantee convergence we are bound to rather small disturbances below the ± 1 rad level.

A possibility that we are exploring is the joint operation with the GS algorithm. Figure 3 illustrates the concept, when the GS is used to reach a rather small residual and then a few iterations of a gradient-based algorithm (here the Fletcher-Reeves algorithm) boost the convergence rate, despite the extra computational cost per iteration.

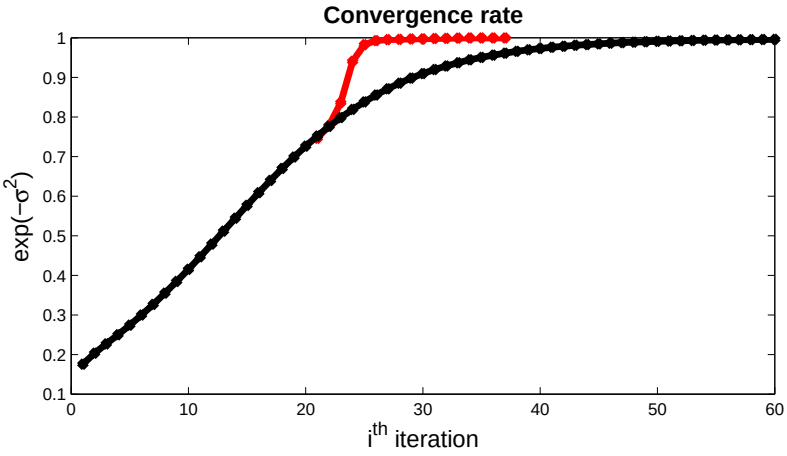

Fig. 3. Convergence rate of the GS algorithm (black). When residuals are small (typically below 1 rad), a few iterations of a gradient-based non-linear minimisation algorithm can boost convergence (red).

In closed-loop, provided the the transient period can be overcome, one could still use a combination of algorithms or a stand alone gradient-based algorithm.

Another possibility, envisioned by ScExAO is to operate behind Subaru's AO188 AO system, thus measuring a partially-corrected wave-front. Such developments are left for future work.

5 Conclusion and Outlook

We present the formalism to deal with any number of images from the `nlCWFS` and we provide a MAP criterion and its derivatives with respect to the parameters of phase. These can then be used with gradient-based non-linear minimisation algorithms. As the explicit computation of the exact derivatives renders the computation in real-time rather cumbersome (at this moment we have a dependence on the number of 2-D FFTs with J, the number of phase parameters), several approximations are required, involving model truncation, linearisation and/or multi-resolution approaches, which are left for future development.

Acknowledgements

The authors acknowledge the support by the European Research Council/European Community under the FP7 through Starting Grant agreement number 239953 and the Marie Curie Intra-European Fellowship grant with reference FP7-PEOPLE-2011-IEF, number 300162. Simulations made with the Object-Oriented Maltab-based AO simulator (OOMAO) freely available from https://github.com/rconan/OOMAO/ .

References

[Correia, 2013] Correia, C. (2013). non-linear curvature wave-front sensor – status report. Technical report, National Research Council of Canada.

[Fienup, 1982] Fienup, J. R. (1982). Phase retrieval algorithms: a comparison. *Appl. Opt.*, 21(15):2758.

[Fienup et al., 1998] Fienup, J. R., Thelen, B. J., Paxman, R. G., and Carrara, D. A. (1998). Comparison of phase diversity and curvature wavefront sensing. volume 3353, pages 930–940. SPIE.

[Guyon, 2010] Guyon, O. (2010). High Sensitivity Wavefront Sensing with a Nonlinear Curvature Wavefront Sensor. , 122:49–62.

[Guyon et al., 2008] Guyon, O., Blain, C., Takami, H., Hayano, Y., Hattori, M., and Watanabe, M. (2008). Improving the sensitivity of astronomical curvature wavefront sensor using dual-stroke curvature. *Publications of the Astronomical Society of the Pacific*, 120(868):pp. 655–664.

[Mahajan, 1998] Mahajan, V. N. (1998). *Optical Imaging and Aberrations - Part I - Ray Geometrical Optics*. SPIE.

[Noll, 1976] Noll, R. J. (1976). Zernike polynomials and atmospheric turbulence. *J. Opt. Soc. Am. A*, 66:207–211.

[Paxman et al., 1992] Paxman, R. G., Schulz, T. J., and Fienup, J. R. (1992). Joint estimation of object and aberrations by using phase diversity. *J. Opt. Soc. Am. A*, 9(7):1072–1085.

[Roddier and Roddier, 1993] Roddier, C. and Roddier, F. (1993). Wave-front reconstruction from defocused images and the testing of ground-based optical telescopes. *J. Opt. Soc. Am. A*, 10(11):2277–2287.